Factors affecting the carbon capture performance of steel slag and green liquor dregs in direct aqueous carbonation

Journal of CO2 Utilization 108 (2026) 103441

Contents lists available at ScienceDirect

Journal of CO2 Utilization

journal homepage: www.elsevier.com/locate/jcou

Factors affecting the carbon capture performance of steel slag and green liquor dregs in direct aqueous carbonation

Eduarda Couto Queiroz [a], Emmanouela Leventaki [a], Alexandre Cuin [b], Björn Haase [c], Christian Kugge [d], Diana Bernin [a,*]

[a] Department of Chemistry and Chemical Engineering, Chalmers University of Technology, Gothenburg 412 96, Sweden
[b] LQBin – Laboratório de Química BioInorgânica, Chemistry Department, Institute of Exact Sciences, Federal University of Juiz de Fora – UFJF, Juiz de Fora, MG 36036-330, Brazil
[c] Höganäs Sweden AB, Bruksgatan 34-35, Höganäs 263 39, Sweden
[d] SCA, R&D Centre, Sundsvall 851 21, Sweden

ARTICLE INFO

Keywords:
Industrial side streams
Carbon dioxide capture
Side stream utilization
Particle size
Porosity

ABSTRACT

Industrial alkaline side streams are attractive candidates for carbon capture via carbonation. Slags from steel manufacturing and dregs from the pulp and paper sector are abundant at industrial sites, offering the potential to offset the carbon dioxide emissions of these sectors. For this process to be techno-economically feasible it is crucial to minimize the energy expense while maximizing the carbonation efficiency. In this work, we studied the carbonation capacity of direct reduced iron slag, ladle furnace slag, electric arc furnace slag and green liquor dregs. Direct aqueous carbonation was conducted with a liquid to solid ratio of 20 L/kg and a gas mixture with 15% carbon dioxide and 85% nitrogen. The impact of three operating parameters was investigated: temperature, particle size and stirring of the mixtures prior to carbonation. It was found that for all the materials higher temperature significantly decreased the carbon dioxide uptake, due to the lower solubility of both carbon dioxide and calcium hydroxide in water. Porosity analysis showed that the steel slags have very low porosity on the micropore scale. Thus, the particle size also had a critical impact in the performance, while the effect was less prominent for green liquor dregs. Similarly, stirring the mixtures prior to carbonation allowed better wetting of the materials and lowering of particle size, which also had a positive effect. This study elucidates the impact of key operating parameters in direct aqueous carbonation with two types of industrial side-streams, and highlights the mechanisms through which they affect the carbonation process.

1. Introduction

Carbon dioxide is the primary anthropogenic greenhouse gas and accounts for the largest share of global greenhouse gas emissions, mainly originating from fossil fuel combustion and industrial flue gas streams. Hence, carbon capture and storage (CCS) is considered to be a necessary measure to mitigate global warming. One effective way to capture and store carbon dioxide is by utilizing materials such as alkaline waste and industrial by-products [1,2]. These materials can capture carbon dioxide through mineral carbonation due to their composition, which includes oxides, hydroxides and silicates of metals such as calcium, magnesium, sodium, potassium and others [1,2]. Furthermore, they offer several advantages, such as high annual production rates, the ability to capture large amounts of carbon dioxide, and the potential for use as construction aggregates after the carbonation reactions [3].

Mineral carbonation reactions occur naturally over long periods of time due to their slow reaction kinetics [4]. To enhance the reaction rate, techniques such as direct and indirect carbonation can be applied. Indirect carbonation is a two-step process that uses an acid pretreatment to extract metals from minerals [5]. Direct carbonation is divided into two types: gas-solid carbonation and aqueous carbonation. In gas-solid carbonation, carbon dioxide in the gas phase reacts with metal oxides in the solid phase under high temperature and pressure. In aqueous carbonation, carbon dioxide is bubbled into water, where it reacts with alkaline metal ions in an aqueous suspension [6].

Direct aqueous carbonation can present several reaction mechanisms, depending on the mineral phases present in the material. Steel slags, the by-products of steel manufacturing, can have a wide range of

* Corresponding author.
E-mail address: diana.bernin@chalmers.se (D. Bernin).

https://doi.org/10.1016/j.jcou.2026.103441
Received 17 December 2025; Received in revised form 3 April 2026; Accepted 23 April 2026
Available online 19 May 2026

mineral phases depending on the type of raw material used in the steel production and the step of the process where the slag is produced. The mineral composition can include a combination of metal oxides, such as calcium and magnesium oxide, calcium silicates, such as C2S ($2CaO{\cdot}SiO_2$), wollastonite ($CaSiO_3$) and larnite (Ca_2SiO_4), calcium magnesium silicates, such as CMS ($CaO{\cdot}MgO{\cdot}SiO_2$) and C3MS2 ($3CaO{\cdot}2MgO{\cdot}SiO_2$), as well as other phases that include iron, manganese and aluminum [7,8].

Green Liquor Dregs (GLD) are another example of an alkaline side-stream from the pulp and paper industry, which is high in calcium and magnesium in the forms of carbonates and hydroxides [9]. The aqueous carbonation process involves the dissolution of metal ions from the hydroxide or silicate phases, dissolution of carbon dioxide in the water and subsequent reaction of the metal ions with the carbonate ions to form carbonates. These reactions for the case of calcium hydroxide and calcium orthosilicate (larnite) are shown in the following equations [10].

Dissolution of carbon dioxide:

$$CO_{2(g)} + H_2O_{(l)} \leftrightarrow H_2CO_{3(aq)} \quad (1)$$

$$H_2CO_{3(aq)} \leftrightarrow HCO^-_{3(aq)} + H^+_{(aq)} \quad (2)$$

$$HCO^-_{3(aq)} \leftrightarrow CO^{2-}_{3(aq)} + H^+_{(aq)} \quad (3)$$

Dissolution of calcium hydroxide and calcium orthosilicate:

$$Ca(OH)_{2(s)} \leftrightarrow Ca^{2+}_{(aq)} + 2OH^-_{(aq)} \quad (4)$$

$$Ca_2SiO_{4(s)} + 4H^+_{(aq)} \leftrightarrow 2Ca^{2+}_{(aq)} + H_2O_{(l)} + SiO_{2(s)} \quad (5)$$

Carbonation:

$$Ca^{2+}_{(aq)} + HCO^-_{3(aq)} \leftrightarrow CaCO_{3(s)} + H^+_{(aq)} \quad (6)$$

$$Ca^{2+}_{(aq)} + CO^{2-}_{3(aq)} \leftrightarrow CaCO_{3(s)} \quad (7)$$

Direct aqueous carbonation presents advantages such as an increased reaction rate, milder reaction conditions, and a higher carbon dioxide absorption capacity when compared to gas-solid carbonation [11]. However, a limitation of this reaction is the leaching of metal ions from minerals. Various techniques have been reported to enhance carbon dioxide absorption, such as the addition of salts (e.g., NaCl, $Na_2C_2O_4$, and $Na_2C_6H_5O_7$) and crushing the minerals to decrease the particle size. The Liquid to Solid ratio (L/S), carbonation temperature, stirring rate and reaction time have also been studied [3,12]. Tu et al. and Zhu et al. studied the accelerated direct aqueous carbonation of steel slags under different experimental conditions. Both found that for L/S ratio of 10 and 15 L/kg, respectively, temperature had a positive effect on the carbonation degree within the range of 20 – 85 °C, although Zhu et al. observed a drop in performance at 45 °C [10,13]. Liu et al. reported that the optimal temperature range is 50 – 60 °C in slurry reactors operating at atmospheric pressure [12].

The influence of temperature and other key process parameters has been widely investigated [10,3,12–14]. However, the majority of studies have been conducted at high partial pressures of carbon dioxide and there is limited work on the effect of lower carbon dioxide inlet concentration [15,16]. To address this, Zhang et al. investigated the effect of inlet carbon dioxide concentration in the range of 10 – 100% during the carbonation of steel slag at a L/S ratio of 10 L/kg [17]. Their results showed that lower concentration significantly slows down the carbonation kinetics, while leading to a slightly higher overall uptake of carbon dioxide. Investigation of carbon dioxide concentration in the range of 10 – 20% is essential to assess the feasibility of directly utilizing flue gas in aqueous carbonation, potentially eliminating the need for prior purification of carbon dioxide. To our knowledge, the combination of elevated temperature and low carbon dioxide concentration has not been reported in direct aqueous carbonation of steel slags.

Unlike steel slags, GLD has not been extensively studied as a material for CO_2 capture, even though its composition includes calcium, magnesium, iron, sodium, potassium and aluminum [18]. GLD is an alkaline waste generated by the pulp and paper industry during the Kraft process. This process uses a mixture of chemicals named white liquor to dissolve lignin and separate cellulose fibers from wood chips [19]. As a result, a mixture of lignin and chemical agents, known as black liquor, is produced. The black liquor is evaporated to concentrate it, forming ~85% black liquor, which is then fed to the recovery boiler to generate energy and to recover the cooking chemicals [20]. During this process, green liquor is formed, which is converted back into white liquor. The insoluble solids that remain after the recovery boiler, the GLD, are typically disposed of in landfills [21]. GLD has been studied for potential use in cement clinker [22], in lightweight aggregates [23] and in sealing layers on mine waste [24]. In a previous study, we investigated the potential of GLD in CCS, where we found a maximum carbon dioxide uptake of 114 g/kg of GLD and the formation of calcite was observed [9]. Thus, we considered that it would be valuable to further explore the carbon capture performance of this material at various process conditions.

GLD and three different steel slags, Petrit T, Petrit E, and Petrit L, from the manufacturing processes of direct reduced iron, electric arc furnace, and ladle furnace, respectively [25], were utilized as materials to capture carbon dioxide. Different temperatures, particle sizes, and stirring time prior to carbonation were analyzed to determine the optimal reaction conditions for enhancing carbon dioxide absorption by the alkaline materials. The L/S ratio (L/kg) of steel slags and GLD was set to 20, as Leventaki et al. and Queiroz et al. reported that this concentration provides maximum carbon dioxide absorption capacity [9,25]. The purpose of this work is to conduct a case study on the direct aqueous carbonation of the investigated materials, building upon our previous work [9,25]. To advance the understanding of their carbonation behavior, a systematic evaluation of the influence of key operating parameters was carried out.

2. Materials and methods

2.1. Materials

Petrit T, Petrit E and Petrit L and their compositions were provided by Höganäs, Sweden. GLD and its composition was given by SCA, Sweden. These are displayed in Table 1.

2.2. Methods

2.2.1. Carbonation experiments

All carbonation experiments were conducted with mixtures of 3 g of each sample and 60 mL of deionized water. The mixtures were stirred for a set amount of time at 400 rpm with a magnetic stirrer at ambient temperature, prior to each run. During the experiments the mixtures were continuously stirred in the same way. The gas flow rate was set to 200 mL/min, comprising 15% carbon dioxide and 85% nitrogen. The flow rate was controlled with mass flow controllers (MFC) and a standalone control panel (0254, Brooks Instrument). The carbon dioxide absorption was monitored using a sensor (ExplorIR, GSS), which

Table 1
Composition of the materials investigated provided by their suppliers.

Composition	Petrit T (%)	Petrit E (%)	Petrit L (%)	GLD (%)
CaO	37	40	48	25
MgO	-	10	13	12.5
SiO_2	18	15	11	1.86
Al_2O_3	9	6.5	9	0.918
FeO	-	25	13	-
Fe_2O_3	7	-	-	0.435

measured the carbon dioxide concentration every 5 s. The reaction was carried out at 1 atm and at a set temperature.

2.2.1.1. Temperature experiments. Mixtures of the samples were prepared as described above. Prior to carbonation the mixtures were stirred for 24 h for Petrit E and L, and 2 h for GLD. During the experiments the temperature of the mixtures was controlled using a water bath equipped with a thermometer. The reaction was carried out at temperatures of 25 °C and 60 °C. Fig. 1 shows the experimental setup. After the reaction, each mixture was dried in an oven at 50 °C for 2 days.

2.2.1.2. Particle size experiments. Mixtures of the samples were prepared as described above. Prior to carbonation the mixtures were stirred for 24 h for Petrit E and L, and 2 h for GLD. The experiments were carried out at 25 °C. For GLD, the experiments were conducted using both the material as received (GLD) and after crushing with a mortar (GLD powder). Petrit E and Petrit L consist of both powder and rocks in their composition; the powder was obtained by sifting the samples through a 1 mm sieve, and experiments were conducted for both powder (Petrit E and Petrit L) and rock particles (Petrit E rocks and Petrit L rocks). Petrit T was provided in powder form and thus was not included in this study. The particle sizes of all samples were calculated from RBG camera images and SEM images which were analyzed with the software FIJI (ImageJ) on a sample size of around 60 particles for each material.

2.2.1.3. Pretreatment stirring time experiments. Mixtures of the samples were prepared and stirred for 2, 4, and 24 h prior to carbonation. After stirring, the mixtures were carbonated in the same way as described above. To corroborate the results from this study sieve analysis was conducted on the steel slags before and after the 24 h stirring pretreatment to evaluate the effect of stirring on the particle size distribution (see supplementary information). The mixtures after 24 h of stirring were placed in an oven at 50 °C for 2 days before the sieve analysis.

To investigate the effect of the stirring time on the leaching of metal ions, samples were stirred for 2, 4, and 24 h, followed by centrifugation at 3000 G for 10 min to separate the precipitates from the solution. The experiments were conducted using the solutions under the same conditions. This was then corroborated with pH measurements on the mixtures during the stirring pretreatment. A pH probe (HQ430D, HACH) was inserted to mixtures of the steel slags prepared in the same way and collected data every 10 s for each steel slag for 24 h.

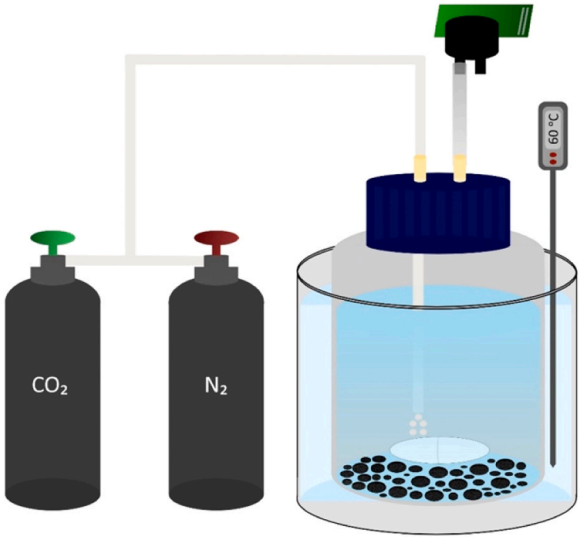

Fig. 1. Diagram of the experimental setup for different temperatures.

2.2.2. Measurement of carbonation yield

The carbon dioxide uptake of each mixture was obtained from the carbon dioxide sensor at the outlet of the reactor. The calculations were done following the publication of Leventaki et al [25]. The sensor was regularly calibrated on the 15% carbon dioxide mixture. During the carbonation experiments it would occasionally display an over- or underestimation of the outlet flow (stabilizing below or above 15%) owing to effects of the temperature, humidity and gradual aging of the sensor's infrared source and optical components. To account for these measurement uncertainties the calculations for all the experiments were conducted based on the maximum output signal of the sensor when the carbon dioxide concentration at the outlet had reached a plateau. The equations are presented below.

Nitrogen outlet flow rate:

$$F_{OUT,\ N_2} = \quad F_{IN,\ N_2} = 200\left(\frac{mL}{\min}\right) * 85\% = 170\left(\frac{mL_{N_2}}{\min}\right) \tag{8}$$

Total outlet flow rate:

$$F_{OUT,\ N_2} + F_{OUT,\ CO_2} = 170\left(\frac{mL_{N_2}}{\min}\right) + \quad F_{OUT,\ CO_2}\left(\frac{mL_{CO_2}}{\min}\right) \tag{9}$$

Outlet concentration of carbon dioxide:

$$CO_2\%_{OUT} = \frac{F_{OUT,\ CO_2}\left(\frac{mL_{CO_2}}{\min}\right)}{170\left(\frac{mL_{N_2}}{\min}\right) + \quad F_{OUT,\ CO_2}\left(\frac{mL_{CO_2}}{\min}\right)} \tag{10}$$

Outlet flow of carbon dioxide:

$$F_{OUT,\ CO_2}\left(\frac{mL_{CO_2}}{\min}\right) = \frac{CO_2\%_{OUT} * 170\left(\frac{mL_{N_2}}{\min}\right)}{1 - CO_2\%_{OUT}} \tag{11}$$

Mass of absorbed carbon dioxide (assuming a gas density of $1.8*10^{-3}$ g / mL throughout all experiments [26]):

$$M_{absorbed\ CO_2} = \left(CO_2\%_{OUT\max} * F_{IN}\left(\frac{mL_{CO_2}}{\min}\right)\right.$$
$$\left. - F_{OUT,\ CO_2}\left(\frac{mL_{CO_2}}{\min}\right)\right) * 5s * \frac{1}{60}\left(\frac{\min}{s}\right) * 0.0018\left(\frac{g}{mL}\right) \tag{12}$$

Thus, the total mass of absorbed carbon dioxide is calculated as the accumulated absorbed mass for the duration of the experiments.

The temperature of the gases was assumed to be ambient during all the carbonation experiments, including the ones where the temperature of the mixture was set to 60 °C. This assumption was made given that the retention time of the gas flow through the reactor was too short for significant heat exchange from the liquid to the gaseous phase. Each carbonation experiment was carried out until the outlet concentration of carbon dioxide would plateau at a value around that of the inlet concentration.

To evaluate the reproducibility of the results some of the carbonation experiments were conducted in duplicate. Also, two carbonated samples were selected for TGA analysis to independently validate the carbon dioxide uptake results using an alternative technique. Based on these results a pooled standard deviation was calculated and applied to all the single measurements, as described by Liengme and Hekman (see Table S1) [27].

2.3. Physicochemical characterization

All four materials were analyzed with a High Throughput Surface Area and Porosity Analyzer (TriStar3000, Micromeritics) to determine their Brunauer–Emmett–Teller (BET) surface area. The adsorbent gas was nitrogen (77 K) and the samples were dried in the SmartPrep instrument (Micromeritics) at 150 °C for 20 h, under nitrogen flow, to remove moisture before the measurement.

To evaluate the stability of the materials during high-temperature degassing, as well as to corroborate the results of carbon dioxide uptake with another technique, samples were subjected to TGA (TGA/DSC 3 + STAR System, Mettler Toledo). The temperature range was 40 – 900 °C with a ramp of 10 °C/min and N_2 flow of 60 mL/min. The yield of carbonation was calculated based on the difference in weight loss between the fresh and carbonated samples within the temperature range of 475 and 800 °C as described in the literature, according to the following equation [28–30].

$$Carbonation\ yield\left(\frac{g_{CO_2}}{kg_{material}}\right) = (\%Weight\ loss_{(475-800^{\circ}C),carbonated\ \ sample} - \%Weight\ loss_{(475-800^{\circ}C),fresh\ \ sample}) \left(\frac{g_{CO_2}}{100g_{material}}\right) * 1000 \left(\frac{g_{material}}{kg_{material}}\right) \quad (13)$$

The morphology of the materials before and after carbonation was studied with SEM (FEI Quanta 200 FEG ESEM) at 20 kV. Energy-Dispersive X-ray Spectroscopy (EDS) was also performed to identify the elemental composition of the different structures. The crystal phases of the materials before and after carbonation were studied with XRD (D8 Discover, Bruker), over a diffraction angle range from 10° to 70° with a step size of 0.04° and counting time of 1 s per step. The QualX2.0 program was used to identify the crystalline phases, and Rietveld analysis was conducted to refine the calculated calcium carbonate polymorph profiles with the experimental XRD data, providing high precision for calcium carbonate polymorphs formed during the carbonation process [31,32].

3. Results and discussion

3.1. Effect of temperature

Fig. 2 shows the carbon dioxide absorption with time for GLD and Petrit T, L and E, at two different temperatures. For GLD at 60°C, the carbon dioxide absorption at the end of the experiment was 0.068 g, which is around 3.5 times lower than the carbon dioxide absorption at 25 °C (0.24 g). For Petrit T, Petrit L, and Petrit E at 60 °C, carbon dioxide absorption values were 0.32 g, 0.30 g, and 0.36 g, respectively, while at 25 °C, they were 0.52 g, 0.56 g, and 0.49 g. This decrease is attributed to the reduction in the solubility of both carbon dioxide and calcium

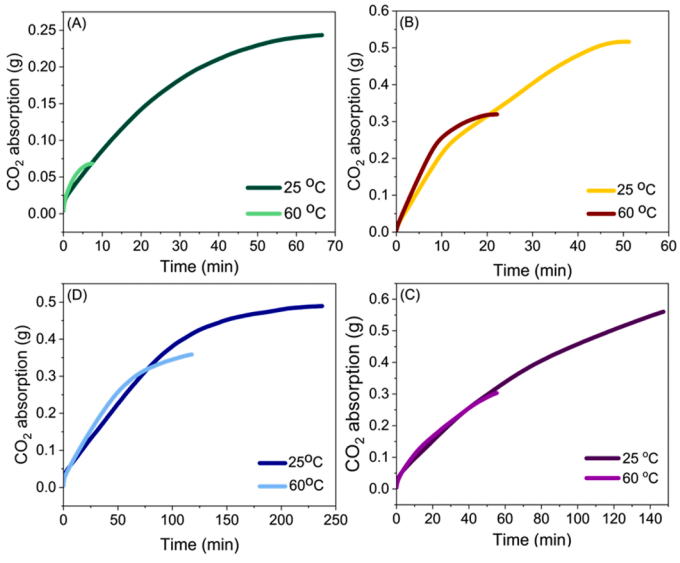

Fig. 2. Carbon dioxide absorption at different temperatures for A) GLD, B) Petrit T, C) Petrit E, and D) Petrit L.

Table 2
Carbon dioxide absorption capacity and yield for GLD, Petrit T, Petrit L, and Petrit E at different temperatures.

	25 °C		60 °C	
	CO_2 (g/L)	CO_2 (g/kg_{solid})	CO_2 (g/L)	CO_2 (g/kg_{solid})
GLD	4.22 ± 0.23	84.3 ± 4.5	1.13 ± 0.13	22.7 ± 2.6
Petrit T	8.59 ± 0.05	171.9 ± 0.9	5.32 ± 0.13	106.5 ± 2.6
Petrit L	9.33 ± 0.13	186.8 ± 2.6	5.04 ± 0.13	101.0 ± 2.6
Petrit E	8.14 ± 0.02	162.9 ± 0.4	5.98 ± 0.13	119.5 ± 2.6

hydroxide. Eq. 14 illustrates the relationship between the solubility of calcium hydroxide and temperature [33]:

$$Ca(OH)_2\ solubility\ (g/kg\ of\ solution) = -0.0108\ T\ (^{\circ}C) + 1.7465 \quad (14)$$

Table 2 shows the carbon dioxide absorption capacity and yield of GLD, Petrit T, L and E at the two different temperatures. This data shows that all materials present the highest carbon dioxide absorption at 25 °C, indicating that room temperature is the optimal between the two temperatures for the carbonation reaction under this experimental setup. This result contradicts the literature in direct aqueous carbonation, which has consistently shown that between 20 and 60 °C there is a positive correlation between the temperature and the carbonation yield [10,13,34]. Interestingly, Francesca Bonfante et al., who performed design of experiment on accelerated carbonation of electric arc furnace slag at L/S ratio of 3, also found a decrease in carbonation with the temperature and concluded that 33 °C was the optimum temperature based on their generated regression model [35]. Based on this, we can speculate that there could be an interaction between the L/S ratio, carbon dioxide inlet concentration, and temperature. In our setup, the lower concentration of carbon dioxide amplifies the importance of carbon dioxide dissolution in the liquid. Calcium silicate has been found to have higher aqueous solubility with increasing temperature [14,36]. Thus, when the inlet gas is almost 100% carbon dioxide, as in accelerated carbonation, higher temperature might overall benefit the carbonation process, by enhancing the availability of calcium ions in solution. At lower carbon dioxide concentration (15%) and higher L/S ratio (20 L/kg) this effect is suppressed by the larger effect of the temperature on the gas dissolution. In the case of GLD, since the silicon content is very low, most of the calcium that is available to react with carbon dioxide would be in the form of calcium hydroxide. This could explain the larger effect of temperature, as both the reactants have a reduction in dissolution at higher temperature.

3.2. Effect of particle size

3.2.1. Particle size

The approximate particle size of GLD, GLD powder, Petrit E, Petrit E rocks, Petrit L, and Petrit L rocks based on image analysis is displayed in Table 3.

3.2.2. BET surface area

The BET surface area of the materials is reported in Table 4. Fig. 3 shows the N_2 isotherms of the three steel slags and the GLD, in both powder and rock form. All the materials presented type II isotherms,

Table 3
Particle size for GLD, GLD powder, Petrit E, Petrit E rocks, Petrit L, and Petrit L rocks.

Size	GLD (mm)	GLD powder (mm)	Petrit E rocks (mm)	Petrit E (mm)	Petrit L rocks (mm)	Petrit L (mm)
Mean	1.1	0.036	6.0	0.28	8.0	0.16
Max	4.5	1.3	1.3	1.0	15.4	0.99
Min	0.24	0.0012	1.6	0.003	1.1	0.005

Table 4
BET surface area of the GLD, GLD powder, Petrit T, Petrit E and Petrit L.

	GLD	GLD powder	Petrit T	Petrit E	Petrit L
BET Surface Area (m^2/g)	34.6	35.9	23.0	2.8	9.5

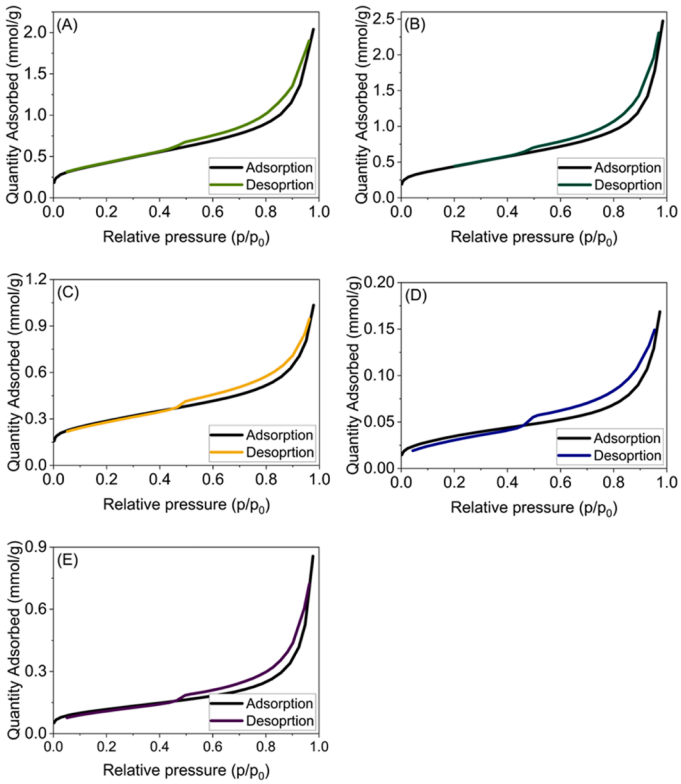

Fig. 3. Physisorption isotherms of (A) GLD, (B) GLD powder, (C) Petrit T, (D) Petrit E and (E) Petrit L.

with hysteresis of type H3, according to the 2025 IUPAC classification [37]. Type II isotherms are characteristic of nonporous or macroporous materials. The H3 type of hysteresis can either indicate the existence of plate-like particles, or the presence of macropores which are not completely filled with pore condensate. Petrit E showed the lowest BET surface area, with 2.8 m^2/g, while GLD, both crushed and not crushed had the highest BET surface area, at 35.9 and 34.6 m^2/g, respectively. The higher BET surface area of GLD suggests that this is the most porous materials of the four, followed by Petrit T, while Petrit L and Petrit E presented significantly lower porosity.

Fig. 4 shows the carbonation yield for different particle sizes of the materials. All the samples exhibit the same pattern: smaller particle sizes have a larger surface area, which enhances the contact between calcium and carbon dioxide. As the particle size increases, the formation of a calcium carbonate layer on the particle surface can hinder the dissolution of more metal hydroxides from within the particle [3].

For GLD, the carbonation yield was 84.3 ± 4.5 g CO_2 / kg material, while GLD powder absorbed 89.6 ± 3.3 g CO_2 / kg material of carbon dioxide. The difference is small, possibly due to its relatively high porosity, which dampens the importance of the particle size. For Petrit E rocks and Petrit L rocks, the carbon dioxide absorption values were 58.2 ± 2.6 g CO_2 / kg material and 126.7 ± 2.6 g CO_2 / kg material, respectively, whereas Petrit E and Petrit L absorbed 163 ± 0.2 g CO_2 / kg material and 186.6 ± 2.6 g CO_2 / kg material, respectively. The difference in carbon dioxide absorption between Petrit E samples was around 64%, and for Petrit L, it is 32%. This falls in line with the results of the BET surface area of the materials, which suggests that the importance of the particle size depends on the porosity of the materials.

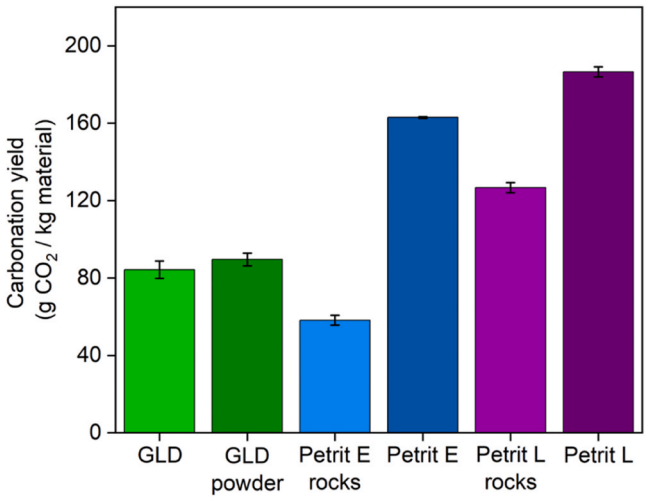

Fig. 4. Carbonation yield for different particle sizes for GLD, GLD powder, Petrit E rocks, Petrit E, Petrit L rocks, and Petrit L.

It is also worth noting that Petrit L contains harder rocks than Petrit E, so that during the stirring pretreatment the Petrit L particles could decrease in size more than the Petrit E ones, as will be discussed below. The same applies for GLD, which is even softer, although, as it was observed above, the surface area of GLD was controlled by the porosity rather than the particle size.

3.3. Stirring time

The mixtures were stirred for 2, 4, and 24 h to compare their carbon dioxide absorption. Increasing the stirring time can reduce the particle size, as the particles collide with the walls of the flask and with each other. Furthermore, stirring for 24 h increases the contact between water and the particles, improving wetting and facilitating the leaching of calcium ions during the reaction. Fig. 5 shows the graphs of carbon dioxide absorption of GLD, Petrit T, Petrit E and Petrit L.

GLD showed small differences in carbonation yield with stirring time with 1.1 times higher yield after 24 h stirring compared to 2 h. For Petrit T, E, and L, however, stirring time appears to be one of the most important parameters. The carbonation yield increased between 2 h of stirring and 24 h by about 1.5 times for Petrit T, 2.2 times for Petrit E, and 2.3 times for Petrit L. The increase in performance could be a result of both the continuous leaching of calcium and magnesium ions and a decrease of the particle size caused by particle collisions during stirring. The difference in particle size distribution for the three steel slags can be observed in Figure S3 and Table S2 shows the D10, D50 and D90 of each sample. All three materials showed a shift to lower particle size after 24 h of stirring. The D50 of Petrit T decreased from 0.050 to 0.042 mm, from 0.396 to 0.370 mm for Petrit E and from 0.144 to 0.059 mm for Petrit L. The D10 decreased from 0.024 mm to 0.006 mm for Petrit T, from 0.066 mm to 0.028 mm for Petrit E and from 0.032 mm to 0.010 mm for Petrit L. Thus, collisions and grinding between the particles during stirring causes a significant decrease in the particle size, which is positive for the carbonation performance.

Leventaki et al. reported the calcium leaching for Petrit T, E, and L at 50 g/L after stirring for 24 h [25]. To further investigate the importance of wetting and leaching, mixtures were stirred for 2, 4 and 24h and centrifuged. The resulting supernatants were subjected to carbonation. Fig. 6 shows the carbon dioxide absorption for the supernatant solutions for all the samples and the absorption of deionized water for comparison.

The carbon dioxide absorption value remained constant, independent of stirring time, suggesting that the solutions were saturated with metal cations already after 2 h of stirring. In the supernatant

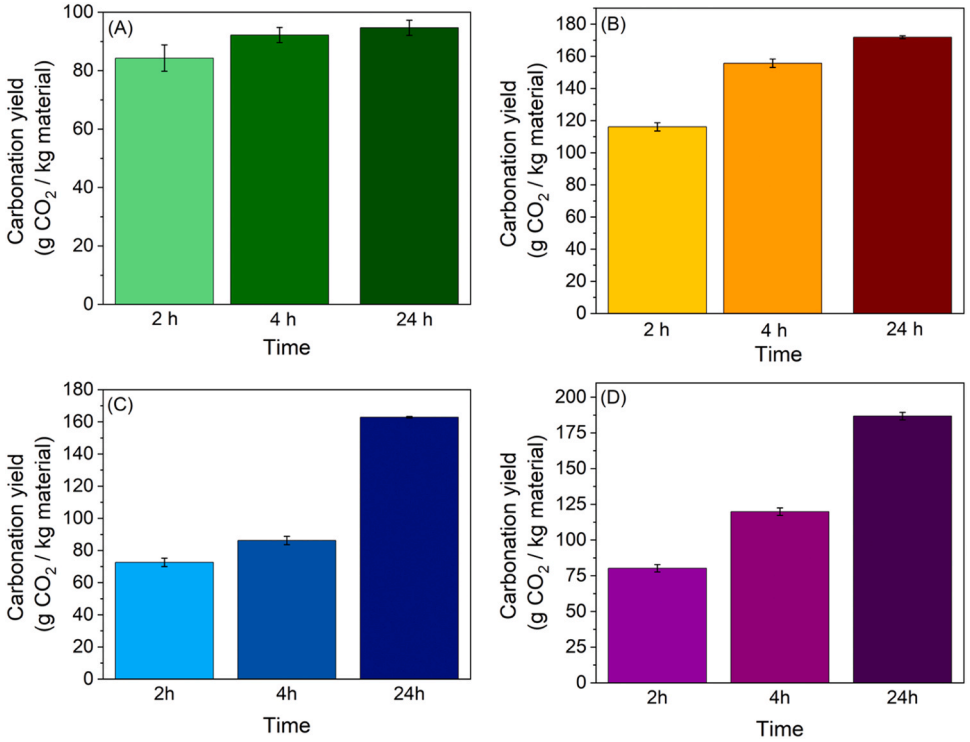

Fig. 5. Carbonation yield from different stirring pretreatment times for (A) GLD, (B) Petrit T, (C) Petrit E and (D) Petrit L.

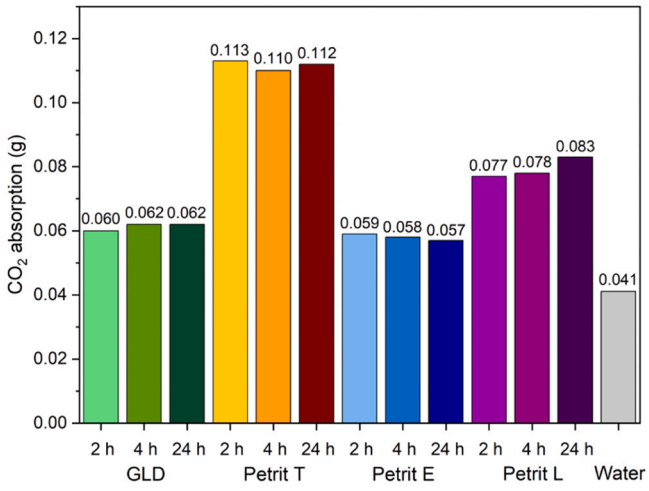

Fig. 6. CO_2 absorption of the supernatant solutions for GLD, Petrit T, Petrit E, and Petrit L after 2, 4, and 24 h of stirring time and of deionized water.

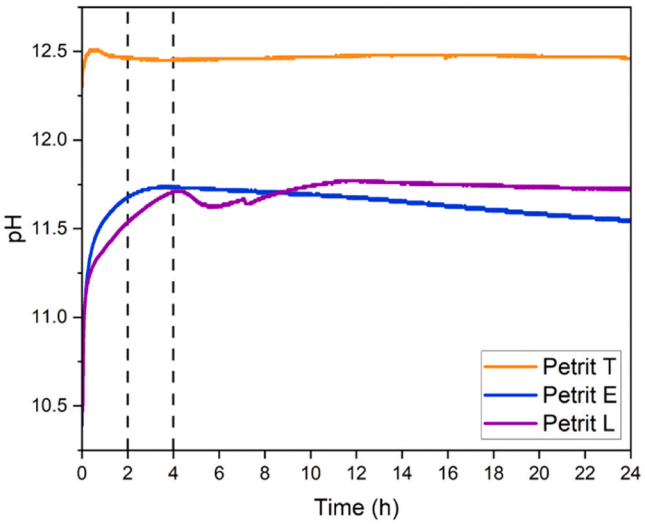

Fig. 7. pH curves of Petrit T, E and L during the stirring pretreatment.

experiments the carbonation was complete within 10 – 22 min, as opposed to the range of 50 – 250 min carbonation experiments of the mixtures. Owing to the very low absorption values of the supernatant solutions, which are comparable to the carbon dioxide absorption in deionized water, it is difficult to reach a conclusion on the effect of the metal ion leaching on the carbonation yield. Thus, samples of steels slags were also stirred for 24 h with the addition of a pH probe that recorded the pH with time. Fig. 7 shows that the pH of the Petrit T mixture increased fast initially from 12.3 to 12.5 and stabilized at around 12.45 within the first 2 h. Petrit E had a slower increase from 10.4 to 11.68 within 2 h, which reached a plateau at 11.7 within 4 h and then slowly drifted downwards to 11.55 after 24 h. Petrit L also had a slow initial increase from 10.5 to 11.5 within 2 h and to 11.7 within 4 h and it finally stabilized at 11.7. This suggests that Petrit E and L have a slower dissolution of metal ions within the first 4 h of stirring, while Petrit T quickly reaches a saturation point in the first 2 h. At 24 h of stirring all slag mixtures had plateaued, yet the low solubility of the metal ions in water limited the absorption capacity of the supernatant solutions. This indicates that calcium leaching during the carbonation process is one of the most important parameters for the carbon dioxide absorption in aqueous direct carbonation. This is because the consumption of calcium ions in solution towards the formation of calcium carbonate drives the dissolution of more calcium ions from the solid phase. Additionally, the lowering of the pH during the carbonation process can facilitate the dissolution of calcium from the various calcium-bearing phases, as the dissolution of calcium ions from calcium hydroxide and silicates is pH driven (see Fig. 8) [38,39].

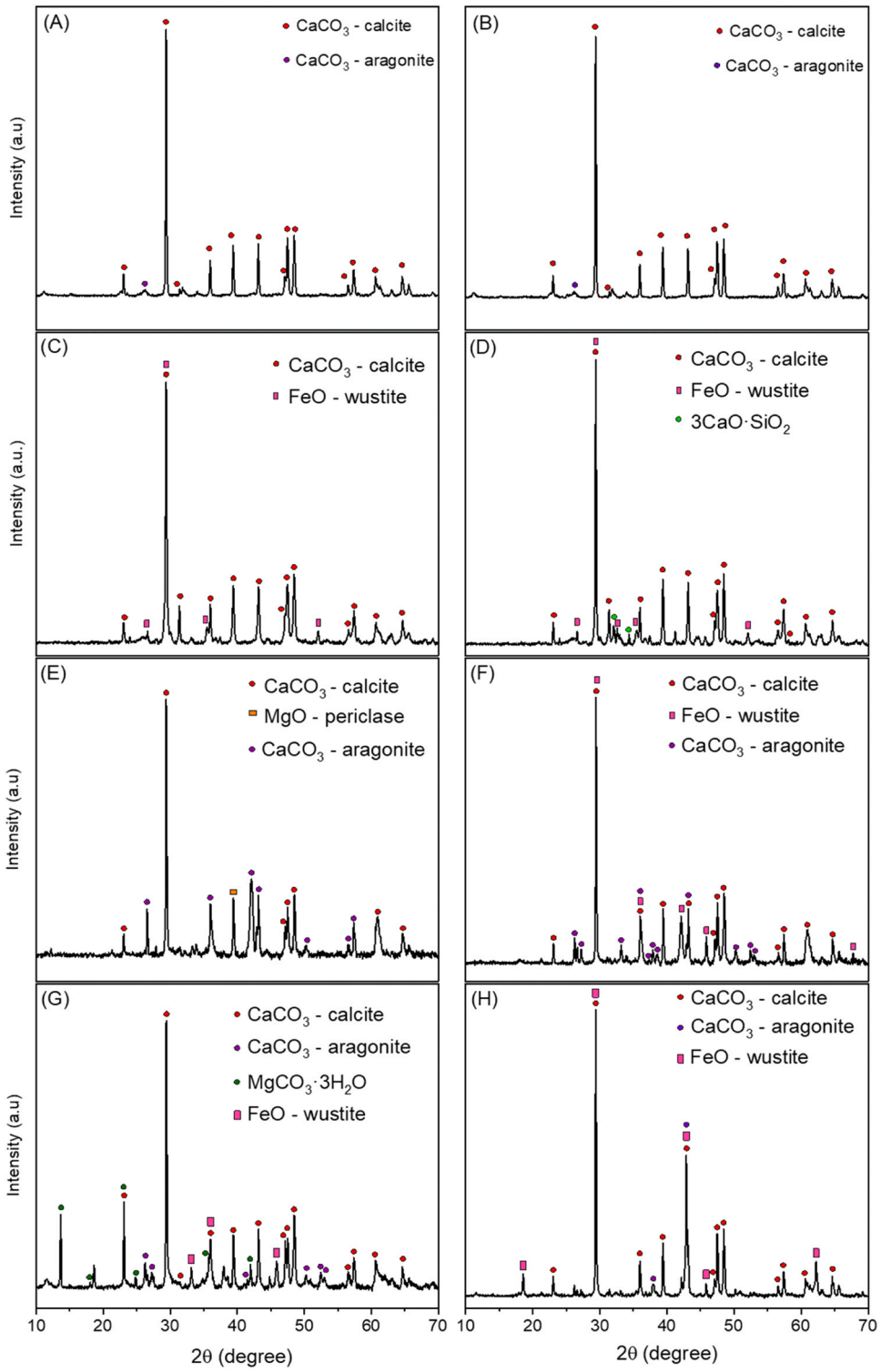

Fig. 8. XRD diffractograms of: GLD at (A) 25°C and (B) 60°C after carbonation, Petrit T at (C) 25°C and (D) 60°C after carbonation, Petrit E at (E) 25°C and (F) 60°C after carbonation and Petrit L at (G) 25°C and (H) 60°C after carbonation.

3.4. XRD analysis

XRD analysis was performed on GLD, Petrit T, Petrit E, and Petrit L samples after carbonation at 25 °C and 60 °C to investigate the impact of temperature on product formation during carbonation (Fig. 8). Calcium carbonate can crystallize in three different morphologies, calcite (cubic), aragonite (needle-like) and vaterite (spherical). Calcite is the most stable polymorph of calcium carbonate, and vaterite is the most unstable, and can become calcite or aragonite in aqueous solution.

For GLD at 25 °C and 60 °C, XRD peaks corresponding to calcite and aragonite were observed (Fig. 8 A, B). The corresponding crystalline phases are presented in supplementary information (Figure S4). For Petrit T at 25 °C and 60 °C, XRD peaks corresponding to calcite and FeO were observed (Fig. 8 C, D). The corresponding crystalline phases are presented in supplementary information (Figure S5). Calcite was the only calcium carbonate polymorph identified in Petrit T. Small peaks

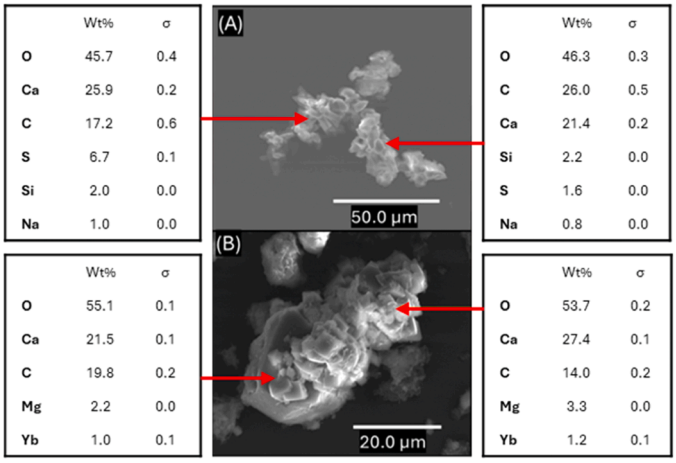

Fig. 9. SEM images for GLD after carbonation at (A) 25 °C and (B) 60 °C.

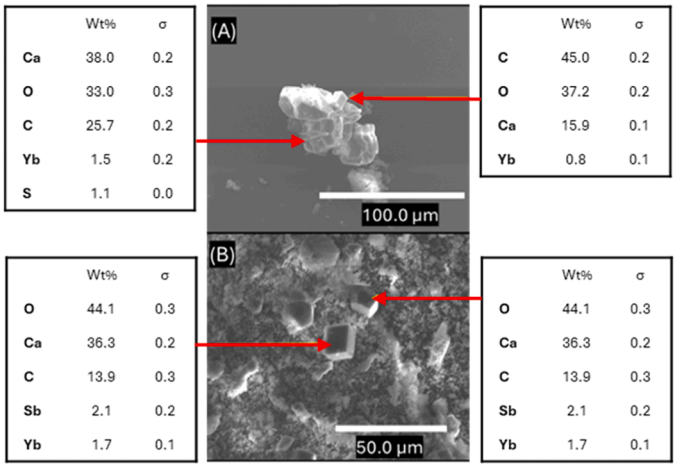

Fig. 10. SEM images for Petrit T after carbonation at (A) 25 °C and (B) 60 °C.

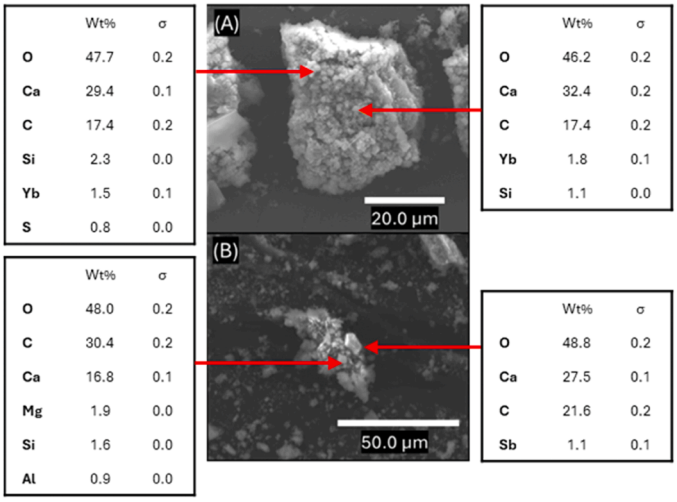

Fig. 11. SEM images for Petrit E after carbonation at (A) 25 °C and (B) 60 °C.

that could be attributed to tricalcium silicate were also observed. For Petrit E at 25 °C and 60 °C, XRD peaks corresponding to calcite, aragonite, and iron(II) oxide were observed (Fig. 8E, F). Additionally, peaks corresponding to magnesium oxide were observed in the XRD pattern at 25 °C. The corresponding crystalline phases are presented in supplementary information (Figure S6). For Petrit L at 25 °C and 60 °C,

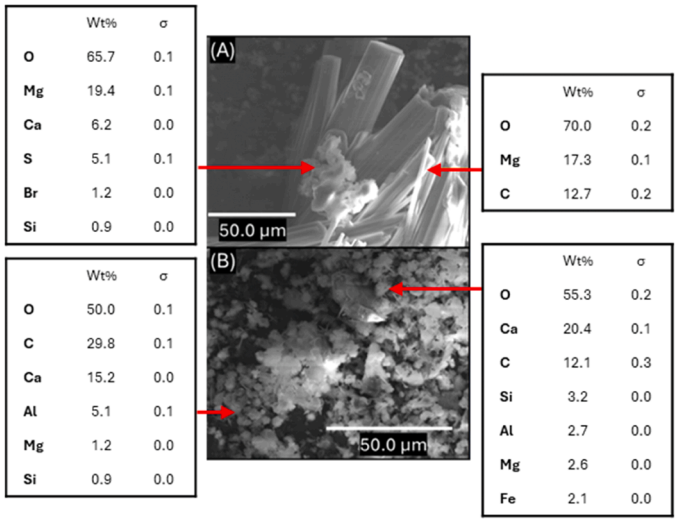

Fig. 12. SEM images for Petrit L after carbonation at (A) 25 °C and (B) 60 °C.

XRD peaks corresponding to calcite, aragonite, and iron(II) oxide were observed (8 G, H). The corresponding crystalline phases are presented in supplementary information (Figure S7). Peaks that could correspond to nesquehonite were identified in the sample of 25 °C, but not in the one of 60 °C. XRD analysis revealed that the formation of calcium carbonate, as crystalline phases of calcite and aragonite, was the predominant outcome of the reaction. No significant differences in calcium carbonate formation were observed between 25 °C and 60 °C.

3.5. SEM analysis

SEM analysis was carried out to analyze the morphology of the samples after carbonation at 25 °C and 60 °C. GLD samples exhibited cubic structures at both temperatures, indicating the formation of calcite (Fig. 9). EDS analysis of these structures revealed that their main components were calcium, oxygen and carbon. A similar square morphology, with a composition of calcium, oxygen and carbon, was observed in Petrit T at 25 °C and 60 °C (Fig. 10).

Petrit E exhibited agglomerates with a cubic morphology made of calcium carbonate, both at 25 °C and 60 °C (Fig. 11). At 25 °C, Petrit L showed a needle-like morphology due to the formation of nesquehonite ($MgCO_3 \cdot 3H_2O$) and an agglomerate of particles composed of oxygen, magnesium, and calcium, suggesting the presence of magnesium hydroxide and calcium hydroxide. At 60 °C, SEM images revealed a needle-like morphology characteristic of aragonite, with the needle structures main composed of calcium, carbon and oxygen (Fig. 12).

4. Conclusions

Four industrial alkaline side streams were evaluated in carbon capture via direct aqueous carbonation: three steel slags with commercial names Petrit T, E and L and GLD from the pulp and paper industry. Several parameters influence the carbonation performance, such as temperature, particle size and pre-carbonation stirring time.

The extend of carbonation was significanly lower at 60 °C compared to 25 °C. The decrease in carbon dioxide capture was approximately 3.59 times for GLD, 1.60 times for Petrit T, 1.36 times for Petrit E, and 1.85 times for Petrit L.

The particle size also had an important effect on the performance. Smaller particles enhance the reaction between calcium hydroxide and carbon dioxide due to their higher surface area. This effect was not as prominent on GLD which is a soft, soil-like material, but it was notable on the steel slags.

The pretreatment stirring time also proved to be a significant factor

in increasing carbon dioxide capture for these materials. Comparing 2 h and 24 h of stirring, the carbon dioxide capture increased by approximately 1.1 times for GLD, 1.5 times for Petrit T, 2.2 times for Petrit E, and 2.3 times for Petrit L.

The pre-carbonation stirring was found to affect both the leaching of calcium and magnesium ions and the particle size distribution of the materials. Sieve analysis showed lower D10, D50 and D90 of the steel slags after 24 h of the stirring pretreatment, while pH monitoring during stirring revealed the time at which each mixture reached a stable pH.

The carbonation process of Petrit T, Petrit E, Petrit L, and GLD demonstrated that the main product formed is calcium carbonate predominantly as calcite. XRD did not reveal significant differences in the product formation between 25 °C and 60 °C. In addition, the formation of nesquehonite was observed for Petrit L.

In summary, optimizing stirring time, particle size, and reaction temperature is essential to maximize calcium carbonate formation and improve the overall efficiency of the carbonation process.

CRediT authorship contribution statement

Eduarda Couto Queiroz: Writing – review & editing, Writing – original draft, Visualization, Methodology, Investigation, Formal analysis, Data curation, Conceptualization. **Christian Kugge:** Writing – review & editing, Resources. **Diana Bernin:** Writing – review & editing, Supervision, Project administration, Funding acquisition. **Alexandre Cuin:** Writing – review & editing, Formal analysis. **Björn Haase:** Writing – review & editing, Resources. **Emmanouela Leventaki:** Writing – review & editing, Visualization, Supervision, Investigation, Formal analysis, Data curation.

Declaration of Competing Interest

The authors declare that they have no known competing financial interests or personal relationships that could have appeared to influence the work reported in this paper.

Acknowledgements

We acknowledge the Area of Advance Energy, Chalmers University of Technology and Energimyndigheten (P2021–00009) for financial support. Authors also thank Carl Tryggers Stiftelse för Vetenskaplig Forskning for providing funding with the project “Instrumentation to utilise research on CO_2 capture to reach the climate goals" (c).

Appendix A. Supporting information

Supplementary data associated with this article can be found in the online version at doi:10.1016/j.jcou.2026.103441.

Data availability

Data will be made available upon request.

References

[1] S.Y. Pan, Y.H. Chen, L.S. Fan, H. Kim, X. Gao, T.C. Ling, P.C. Chiang, S.L. Pei, G. Gu, CO2 mineralization and utilization by alkaline solid wastes for potential carbon reduction, Nat. Sustain 3 (2020) 399–405, https://doi.org/10.1038/s41893-020-0486-9.

[2] F.M. Baena-Moreno, E. Leventaki, A. Riddell, J. Wojtasz-Mucha, D. Bernin, Effluents and residues from industrial sites for carbon dioxide capture: a review, Environ. Chem. Lett. (2022), https://doi.org/10.1007/s10311-022-01513-x.

[3] X. Huang, J. Zhang, L. Zhang, Accelerated carbonation of steel slag: A review of methods, mechanisms and influencing factors, Constr. Build. Mater. 411 (2024) 134603, https://doi.org/10.1016/j.conbuildmat.2023.134603.

[4] N. Thonemann, L. Zacharopoulos, F. Fromme, J. Nühlen, Environmental impacts of carbon capture and utilization by mineral carbonation: A systematic literature review and meta life cycle assessment, J. Clean. Prod. 332 (2022) 130067, https://doi.org/10.1016/j.jclepro.2021.130067.

[5] Y. Luo, D. He, Indirect carbonation by a two-step leaching process using ammonium chloride and acetic acid, Jom 74 (2022) 1958–1968, https://doi.org/10.1007/s11837-022-05217-z.

[6] E.R. Bobicki, Q. Liu, Z. Xu, H. Zeng, Carbon capture and storage using alkaline industrial wastes, Prog. Energy Combust. Sci. 38 (2012) 302–320, https://doi.org/10.1016/j.pecs.2011.11.002.

[7] G. Ren, Z. Guo, Influence of phase composition on steel slag flue gas desulfurization performance and controlled enhancement, Ind. Eng. Chem. Res. 62 (2023) 21750–21759, https://doi.org/10.1021/acs.iecr.3c03628.

[8] I.Z. Yildirim, M. Prezzi, Chemical, mineralogical, and morphological properties of steel slag, Adv. Civ. Eng. 2011 (2011) 1–13, https://doi.org/10.1155/2011/463638.

[9] E. C. Queiroz, E. Leventaki, C. Kugge, D. Bernin, CO $_2$ Capture through Aqueous Carbonation Using Green Liquor Dregs as the Absorbent, ACS Sustain. Resour. Manag. 2 (2025) 119–126, https://doi.org/10.1021/acssusresmgt.4c00373.

[10] M. Tu, H. Zhao, Z. Lei, L. Wang, D. Chen, H. Yu, T. Qi, Aqueous Carbonation of Steel Slag: A Kinetics Study, ISIJ Int. 55 (2015) 2509–2514, https://doi.org/10.2355/isijinternational.ISIJINT-2015-142.

[11] X. Lin, Y. Zhang, H. Liu, G. Boczkaj, Y. Cao, C. Wang, Carbon dioxide sequestration by industrial wastes through mineral carbonation: Current status and perspectives, J. Clean. Prod. 434 (2024) 140258, https://doi.org/10.1016/j.jclepro.2023.140258.

[12] X. Liu, X. Ai, Z. Que, X. Liu, Z. Zhang, A review of steel slag carbonation: mechanisms, applications, and sustainability assessment, Materials 19 (2026) 286, https://doi.org/10.3390/ma19020286.

[13] F. Zhu, L. Cui, Y. Liu, L. Zou, J. Hou, C. Li, G. Wu, R. Xu, B. Jiang, Z. Wang, Experimental investigation and mechanism analysis of direct aqueous mineral carbonation using steel slag, Sustainability 16 (2023) 81, https://doi.org/10.3390/su16010081.

[14] X. Zhang, J. Zhao, Y. Liu, J. Li, Use of steel slag as carbonation material: A review of carbonation methods and evaluation, environmental factors and carbon conversion process, J. CO2 Util. 88 (2024) 102947, https://doi.org/10.1016/j.jcou.2024.102947.

[15] J. Liu, C. Zeng, Z. Li, G. Liu, W. Zhang, G. Xie, F. Xing, Carbonation of steel slag at low CO2 concentrations: Novel biochar cold-bonded steel slag artificial aggregates, Sci. Total Environ. 902 (2023) 166065, https://doi.org/10.1016/j.scitotenv.2023.166065.

[16] A.Ben Ghacham, L.-C. Pasquier, E. Cecchi, J.-F. Blais, G. Mercier, CO2 sequestration by mineral carbonation of steel slags under ambient temperature: parameters influence, and optimization, Environ. Sci. Pollut. Res. 23 (2016) 17635–17646, https://doi.org/10.1007/s11356-016-6926-4.

[17] D. Zhang, J. Jiang, J. Zhou, Y. Weng, J. Lan, P. Zhang, D. Wang, Aqueous carbonation of steel slag with different CO2 concentration for the application of supplementary cementitious materials, Sustain. Chem. Pharm. 48 (2025) 102239, https://doi.org/10.1016/j.scp.2025.102239.

[18] F. Martins, J. Martins, L. Ferracin, C. Dacunha, Mineral phases of green liquor dregs, slaker grits, lime mud and wood ash of a Kraft pulp and paper mill, J. Hazard. Mater. 147 (2007) 610–617, https://doi.org/10.1016/j.jhazmat.2007.01.057.

[19] K. Manskinen, H. Nurmesniemi, R. Pöykiö, Total and extractable non-process elements in green liquor dregs from the chemical recovery circuit of a semi-chemical pulp mill, Chem. Eng. J. 166 (2011) 954–961, https://doi.org/10.1016/j.cej.2010.11.082.

[20] T. Kinnarinen, M. Golmaei, E. Jernström, A. Häkkinen, Separation, treatment and utilization of inorganic residues of chemical pulp mills, J. Clean. Prod. 133 (2016) 953–964, https://doi.org/10.1016/j.jclepro.2016.06.024.

[21] M. Golmaei, T. Kinnarinen, E. Jernström, A. Häkkinen, Study on the filtration characteristics of green liquor dregs, Chem. Eng. J. 317 (2017) 471–480, https://doi.org/10.1016/j.cej.2017.02.104.

[22] S. Srivastava, S. Moukannaa, V. Isteri, D.D. Ramteke, P. Perumal, D. Adesanya, P. Kinnunen, K. Ohenoja, M. Illikainen, Utilization of calcite-rich Green Liquor Dregs (GLD) by-products from pulp and paper industry: Cement clinker production and life cycle analysis, Case Stud. Constr. Mater. 20 (2024) e02870, https://doi.org/10.1016/j.cscm.2024.e02870.

[23] E. Adesanya, J. Yliniemi, P. Kinnunen, M. Finnilä, M. Illikainen, Utilization of green liquor dreg in lightweight aggregates: Effect of texture on physical properties, Dev. Built Environ. 15 (2023), https://doi.org/10.1016/j.dibe.2023.100219.

[24] M. Mäkitalo, C. Maurice, Y. Jia, B. Öhlander, Characterization of Green Liquor Dregs, Potentially Useful for Prevention of the Formation of Acid Rock Drainage, (2014) 330–344. https://doi.org/10.3390/min4020330.

[25] E. Leventaki, E. Couto Queiroz, S. Krishnan Pisharody, A. Kumar Siva Kumar, P. Hoang Ho, M. Andersson-Sarning, B. Haase, F.M. Baena-Moreno, A. Cuin, D. Bernin, Aqueous mineral carbonation of three different industrial steel slags: Absorption capacities and product characterization, Environ. Res. 252 (2024) 118903, https://doi.org/10.1016/j.envres.2024.118903.

[26] 2018, Carbon dioxide-Density and Specific Weight vs. Temperature and Pressure. The Engineering ToolBox.(accessed December 9, 2023)2018https://www.engineeringtoolbox.com/carbon-dioxide-density-specific-weight-temperature-pressure-d_2018.html.

[27] B. Liengme, K. Hekman, Statistics for Experimenters. Liengme’s Guide to Excel® 2016 for Scientists and Engineers, Elsevier, 2020, pp. 371–396, https://doi.org/10.1016/B978-0-12-818249-9.00016-9.

[28] C. Crouzet, F. Brunet, G. Montes-Hernandez, N. Recham, N. Findling, J.-H. Ferrasse, B. Goffé, Hydrothermal Valorization of Steel Slags—Part I: Coupled H2

Production and CO2 Mineral Sequestration, Front. Energy Res. 5 (2017), https://doi.org/10.3389/fenrg.2017.00029.
[29] L. Zhao, D. Wu, W. Hu, J. Li, Z. Zhang, F. Yang, Z. Wang, W. Ni, Coupling Mineralization and Product Characteristics of Steel Slag and Carbon Dioxide, Minerals 13 (2023) 795, https://doi.org/10.3390/min13060795.
[30] N. Zhang, G. Deng, W. Liao, H. Ma, C. Hu, Aqueous carbonation of steel slags: A comparative study on mechanisms, Cem. Concr. Compos 155 (2025) 105838, https://doi.org/10.1016/j.cemconcomp.2024.105838.
[31] A. Altomare, N. Corriero, C. Cuocci, A. Falcicchio, A. Moliterni, R. Rizzi, *QUALX2.0*: a qualitative phase analysis software using the freely available database POW_COD, J. Appl. Crystallogr 48 (2015) 598–603, https://doi.org/10.1107/S1600576715002319.
[32] P. Paufler, R. A. Young (ed.). The Rietveld Method. International Union of Crystallography. Oxford University Press 1993. 298 p. Price £ 45.00. ISBN 0–19–855577–6, 494–494, Cryst. Res. Technol. 30 (1995), https://doi.org/10.1002/crat.2170300412.
[33] S.-J. Han, M. Yoo, D.-W. Kim, J.-H. Wee, Carbon dioxide capture using calcium hydroxide aqueous solution as the absorbent, Energy & Fuels 25 (2011) 3825–3834, https://doi.org/10.1021/ef200415p.
[34] S.-Y. Pan, T.-C. Chung, C.-C. Ho, C.-J. Hou, Y.-H. Chen, P.-C. Chiang, CO2 Mineralization and Utilization using Steel Slag for Establishing a Waste-to-Resource Supply Chain, Sci. Rep. 7 (2017) 17227, https://doi.org/10.1038/s41598-017-17648-9.
[35] F. Bonfante, G. Ferrara, P. Humbert, D. Garufi, J.-M. Tulliani, P. Palmero, Direct aqueous carbonation of electric arc furnace slag: process optimisation through experimental design, Mater. Struct. 58 (2025) 127, https://doi.org/10.1617/s11527-025-02661-6.
[36] Y. Li, H. Pan, Z. Li, Unravelling the dissolution dynamics of silicate minerals by deep learning molecular dynamics simulation: A case of dicalcium silicate, Cem. Concr. Res. 165 (2023) 107092, https://doi.org/10.1016/j.cemconres.2023.107092.
[37] M. Thommes, K. Kaneko, A.V. Neimark, J.P. Olivier, F. Rodriguez-Reinoso, J. Rouquerol, K.S.W. Sing, Physisorption of gases, with special reference to the evaluation of surface area and pore size distribution (IUPAC Technical Report), Pure Appl. Chem. 87 (2015) 1051–1069, https://doi.org/10.1515/pac-2014-1117.
[38] G.M.N. Baston, A.P. Clacher, T.G. Heath, F.M.I. Hunter, V. Smith, S.W. Swanton, Calcium silicate hydrate (C-S-H) gel dissolution and pH buffering in a cementitious near field, Mineral. Mag. 76 (2012) 3045–3053, https://doi.org/10.1180/minmag.2012.076.8.20.
[39] B. Kutus, A. Gácsi, A. Pallagi, I. Pálinkó, G. Peintler, P. Sipos, A comprehensive study on the dominant formation of the dissolved Ca(OH) $_{2(aq)}$ in strongly alkaline solutions saturated by Ca(<scp>ii</scp>), RSC Adv. 6 (2016) 45231–45240, https://doi.org/10.1039/C6RA05337H.